Kinetics of Charge Carriers across a Graphene-Silicon Schottky Junction

Mohammad Javadi,* Aliakbar Noroozi, and Yaser Abdi
Department of Physics, University of Tehran, Tehran 14395-547, Iran

(Received 13 September 2020; revised 8 November 2020; accepted 18 November 2020; published 15 December 2020)

We perform a comparative study on the transfer velocity of charge carriers across two-dimensional and (2D) three-dimensional (3D) graphene-silicon and 3D-3D Au-silicon Schottky junctions. Within the framework of classical thermionic emission theory, the transfer velocity of carriers across the Au-Si interface is determined as $\bar{v} \sim 10^7$ cm/s that is thoroughly consistent with the average thermal velocity of carriers in silicon. In contrast, the graphene-Si interface discloses a much lower transfer velocity of $\bar{v} \sim 10^1$ cm/s, i.e., nearly 6 orders of magnitude smaller than the thermal velocity of carriers in silicon. Utilizing the T^1 universal scaling law for vertical 2D-3D Schottky junctions, we determine the effective out-of-plane velocity of charge carriers in graphene as $v_\perp^* \sim 10^0$ cm/s. This indicates current flow across the graphene-Si contact is substantially limited by $v_\perp^*$. Moreover, by analyzing experimental activation-energy data, we uncover a general correlation between the kinetics of charge carriers and the potential barrier at the graphene-Si interface. It is found that the transfer velocity increases almost exponentially with the Schottky barrier height, which cannot be explained in the framework of classical theory. Considering nonconserving $\mathbf{k}_\parallel$ scattering strength as an exponential function of Schottky barrier height, T^1 scaling theory leads to a comprehensive interpretation of experimental data. This study sheds light on the electronic processes across 2D-3D interfaces.

DOI: 10.1103/PhysRevApplied.14.064048

I. INTRODUCTION

Integration of two-dimensional (2D) materials into CMOS technology may supply new device concepts with higher performance and lower energy consumption [1,2]. As a prototype class of 2D and three-dimensional (3D) hybridization, the graphene-semiconductor heterojunctions [3] like graphene-Si and graphene-GaAs have been intensively studied in a variety of electronic and optoelectronic applications, including solar cells [4–8], diodes [9–11], triodes [12], photodetectors [13–17], and optical modulators [18,19]. The phenomenon of charge carrier transport across the 2D-3D interface has also been critically investigated as it plays the central role in the overall performance of hybrid devices [20–24].

At high enough temperatures, current flow through the graphene-Si rectifiers is dominated by thermionic emission of charge carriers over the Schottky barrier at the 2D-3D interface. There is a general agreement among experimental observations that the thermionic emission prefactor (Richardson constant) across the graphene-Si Schottky junction is much lower than the theoretical value predicted by the classical thermionic emission theory [21, 25–30]. Physically, it means that the transfer velocity of carriers across the graphene-Si interface is very low. Charge-carrier transfer across non-Ohmic (semi)metal-semiconductor junctions is essentially determined by the carrier kinetics and the interface barrier height. From the energy perspective, only those carriers with sufficiently high kinetic energy may pass the potential barrier and contribute to the net current flow through the system. The effect of interface barrier height on the charge transport as well as the performance of graphene-Si Schottky devices is well established in previous studies [21–30]. However, the role of charge-carrier kinetics has received little experimental attention.

In this paper, we study the kinetics of charge carriers across the graphene-Si interface. Experimental investigations are carried out through activation-energy measurements. The average transfer velocity of charge carriers across 2D-3D graphene-Si Schottky junctions is extracted and compared with a control device of the Au-Si Schottky junction as a 3D-3D interface. The experimental data are interpreted with regard to classical thermionic emission theory and the new formalism of the T^1 universal scaling law [20]. Furthermore, activation-energy data are collected into a unit frame and a strong correlation between charge-carrier transfer velocity and the interface barrier height is uncovered. This connection explains the broad distribution of the (experimentally extracted) Richardson constant across the graphene-Si interface [21,25–30]. The presence of a thin interfacial silicon suboxide layer at the

*m_javadi_b@ut.ac.ir

 © 2020 American Physical Society

graphene-Si interface is approved experimentally and its effect on the carrier injection velocity is presented. We discuss the failure of classical thermionic emission theory in the evaluation of carriers velocity at 2D-3D Schottky junctions. Finally, we show that by considering an exponential dependence of lateral-momentum scattering strength on the Schottky barrier height, the T^1 scaling formalism can successfully interpret the kinetics of charge carriers at the 2D-3D interface.

II. EXPERIMENT

Graphene-silicon Schottky devices are fabricated in a similar manner to our previous report [31]. In brief, lightly n-doped (1–10 Ω cm) silicon pieces with a 300-nm buffer layer are patterned on the selected square-shape regions and subsequently the buffer sublayers are removed by wet chemical etching. In order to prevent surface oxidation, the silicon samples are kept in nitrogen atmosphere prior to the transformation of graphene (CVD-graphene, Graphenea). Two graphene-Si samples with an active contact area of $A = 0.225$ cm^2 [G-Si(1)] and $A = 0.063$ cm^2 [G-Si(2)] are fabricated and studied. An Au(400 nm)-Si diode as a 3D-3D Schottky junction with a contact area of $A = 0.225$ cm^2 is also fabricated in the same manner and studied for comparison [32]. In order to acquire activation-energy data, current-voltage characteristics of the Schottky junctions are measured in darkness and in a broad range of temperatures from 250 to 430 K. Figure 1 shows schematic representations and typical current density versus voltage characteristics of Au-Si and G-Si Schottky junctions.

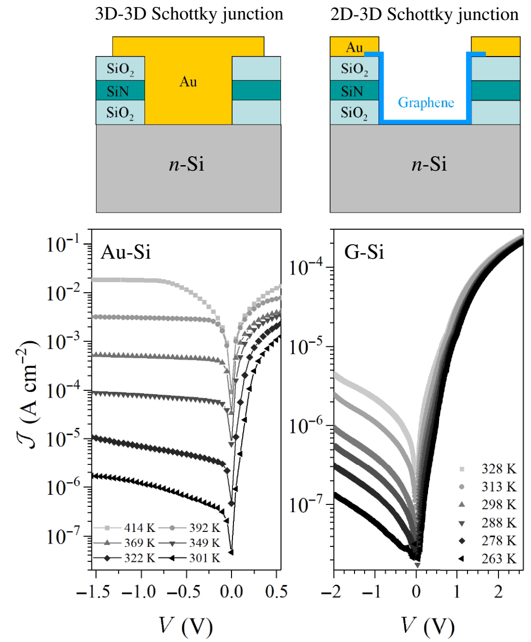

FIG. 1. Schematic representation and dark current-voltage characteristics of Au-Si and G-Si Schottky junctions measured at different temperatures.

III. RESULTS AND DISCUSSION

A. Classical approach

Figure 2(a) represents the energy band diagram at the graphene-silicon interface. Current flow across the Schottky junctions is governed by $\mathcal{J} = \mathcal{J}_0[\exp(qV/k_BT) - 1]$, where the reverse saturation current is determined through the kinetics of charge carriers and the interface barrier height as [33,34]

$$\mathcal{J}_0 = \frac{1}{4}q\bar{v}n = \frac{1}{4}q\bar{v}N_c \exp\left(-\frac{q\varphi_B}{k_BT}\right). \quad (1)$$

In the above equation, q, $\bar{v}$, and n are the elementary charge, average transfer velocity of carriers across the interface, and the density of charge carriers contributing to the current flow, respectively. k_B and T are the Boltzmann constant and absolute temperature, N_c is the effective density of states at the conduction-band edge of the semiconductor, and φ_B is the Schottky barrier height at the interface. Equation (1) provides a practical approach to determine both the carrier kinetics and the interface barrier height. At reverse bias, $\ln(|\mathcal{J}|)$ vs q/k_BT can be fitted by a linear regression whose slope and intercept are given by $-\varphi_B$ and $\ln(q\bar{v}N_c/4)$, respectively.

Figure 2(b) shows typical activation-energy data of the three samples. From the slope of the regression lines fitted to the Au-Si data, we obtain a *zero-bias* Schottky barrier height of $q\varphi_B = 1.01(\pm 0.05)$ eV [32]. Considering the electron affinity of silicon ($q\chi_{\text{Si}} = 4.05$ eV) and the work function of Au ($q\phi_{\text{Au}} = 5.1$ eV), from the Schottky-Mott rule one expects a barrier height of $q\varphi_B = q(\phi_{\text{Au}} - \chi_{\text{Si}}) = 1.05$ eV for the Au-Si Schottky junction. Hence, the measured barrier height is in good agreement with theory. For the G-Si samples we get a barrier height of 0.42–0.46 eV [32] implying that the work function of graphene in the graphene-silicon system is in the range of 4.47–4.51 eV, which is very close to the work function of single-layer graphene [35].

Using $N_c = 2.8 \times 10^{19}$ cm^{-3} for the conduction band of silicon, we determine the average transfer velocity of charge carriers from the intercept of the regression lines [Fig. 2(b)]. For the 3D-3D Au-silicon Schottky junction, the average transfer velocity is obtained as $\langle \bar{v}_{\text{Au-Si}} \rangle = 1.04(\pm 0.03) \times 10^7$ cm/s, which is consistent with the average thermal velocity of charge carriers in silicon. From the Maxwell-Boltzmann distribution, the average thermal velocity of carriers is given by $\langle v_{\text{th}} \rangle = \sqrt{8k_BT/\pi m^*}$. Substituting the density-of-states' effective mass of carriers in silicon, we find $\langle v_{\text{th}} \rangle = 1.9 \times 10^7$ cm/s. On the other hand, the 2D-3D graphene-silicon Schottky junctions display much lower transfer velocity as $\langle \bar{v}_{\text{G-Si(1)}} \rangle = 41.33(\pm 2.22)$ cm/s and $\langle \bar{v}_{\text{G-Si(2)}} \rangle =$

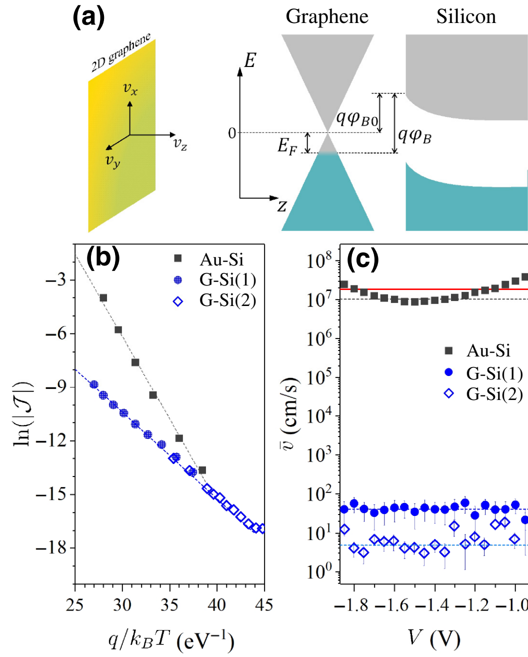

FIG. 2. (a) Schematic representation of velocity axes in 2D graphene sheet and energy band diagram at graphene-Si interface. (b) Classical activation-energy characteristics of Au-Si and G-Si Schottky junctions at $V = -1$ V. (c) Charge transfer velocity versus the reverse bias voltage. Red line shows the average thermal velocity of carriers in silicon $\langle v_{\rm th}\rangle$.

4.78($\pm$0.57) cm/s, almost 6 orders of magnitude lower than the average thermal velocity of carriers in silicon. This is in accord with the previous reports on the low Richardson constant across the graphene-Si interface. Richardson constant is given by $A^* = 4\pi q m^* k_B^2/h^3$, where m^* is the effective mass of carriers in the semiconductor. Taking into account the impact of quantum-mechanical tunneling and reflection at the interface, the effective Richardson constant for n-Si is determined as $A^{**} \approx 110$ A cm^{-2} K^{-2} [34]. However, experimental studies on the graphene-Si Schottky junction indicate two distinctive characteristics [21,25–30]. First, the typical value of the Richardson constant is much smaller than 110 A cm^{-2} K^{-2}. Second, the extracted values show a rather broad distribution ranging from 10^{-9} to 10^1 A cm^{-2} K^{-2}.

B. Ang formalism (T^1 scaling)

In the framework of classical theory, the *thermionic emission prefactor* across the 3D–3D Schottky junction is solely determined through the electronic properties of the semiconductor. In contrast, there is growing evidence that charge transport across the 2D–3D Schottky junction is mostly determined by the electronic properties of the 2D material [20–22,31,36–39]. According to the new formalism developed by Ang and colleagues [20,40–43], current flow across the vertical graphene-semiconductor Schottky junction belongs to a different universal class (T^1 scaling) within which the reverse saturation current is given by

$$\mathcal{J}_0 = \mathcal{C}_{\mathcal{G}}(q\varphi_B)v_\perp^* T\exp\left(-\frac{q\varphi_B}{k_BT}\right). \quad (2)$$

Here $\mathcal{C}_{\mathcal{G}}$ is a constant related to the electronic properties of graphene

$$\mathcal{C}_{\mathcal{G}} = \frac{g_{\rm sv}qk_B}{2\pi l_\perp \hbar^2 v_F^2} \approx 0.06 \quad \text{C/eVcm}^3\text{K}, \quad (3)$$

where $g_{\rm sv} = 4$ is the spin-valley degeneracy, $l_\perp = 0.335$ nm is the thickness of graphene layer, and $v_F = 10^8$ cm/s is the Fermi velocity. $v_\perp^*$ is the *effective out-of-plane velocity* of charge carriers in graphene and is related to the out-of-plane velocity ($v_\perp$) through nonconserving $\mathbf{k}_\parallel$ scattering strength as $v_\perp^* = \lambda_{\mathbf{k}_\parallel} v_\perp$. Utilizing a finite quantum-well model and for the relevant Schottky barrier heights in semiconductor heterostructures (e.g., 0.5 eV), the out-of-plane velocity is determined as $v_\perp = 3.7 \times 10^8$ cm/s [20].

Charge-carrier scattering at the interface may considerably affect the out-of-plane velocity. In this regard, the total current density can be expressed as the sum of two ingredients related to the conserving $\mathbf{k}$ and nonconserving $\mathbf{k}$ components [44,45]. In the case of lateral-momentum conservation, only a small fraction of charge carriers with sufficiently high perpendicular kinetic energy may overcome the interface barrier. In comparison, if the lateral momentum is not conserved, the number of charge carriers contributing to the current flow over the Schottky barrier increases considerably. In this case, the out-of-plane velocity is modified as $v_\perp \to \lambda_{\mathbf{k}_\parallel} v_\perp$. For graphene, it is shown that if the width of the depletion region is larger than 1 nm, the nonconserving $\mathbf{k}_\parallel$ component will dominate the total current density [20]. The previous criteria is fully satisfied for graphene-semiconductor Schottky junctions except for the heavily doped semiconductors ($>10^{19}$ cm^{-3}).

1. Kinetics of charge carriers in two dimensions

It is noted that $\mathcal{J}_0 = q\bar{v}n/4$ in Eq. (1) is derived from the statistical kinetics of particles in three dimensions [46]. Substituting $N_c = 2(2\pi m^* k_B T/h^2)^{3/2}$ and $\langle v_{\rm th}\rangle = \sqrt{8k_BT/\pi m^*}$ into the rhs of Eq. (1), one readily obtains the saturation current of 3D-3D Schottky junction as $\mathcal{J}_0 = A^*T^2\exp(-q\varphi_B/k_BT)$. In two dimensions, the statistical kinetics of charge carriers leads to Eq. (2). Let us assume that the distribution of carrier velocity in two-dimensional graphene is given by $\mathcal{F}(\vec{v})$ with $\vec{v} = \vec{v}(v_x, x_y)$ and a normalization condition of $\int_0^\infty \mathcal{F}(\vec{v})d\vec{v} = 1$ [see Fig. 2(a)]. In the out-of-plane direction, the graphene sheet can be considered as a finite potential well leading to quantized energy and momentum bound states in $\hat{z}$ direction.

Alternatively, due to the position-momentum uncertainty $\Delta z \Delta p_z \sim \hbar$, charge carriers in graphene always possess a nonzero velocity component in the out-of-plane direction ($\Delta z = l_\perp$ being the thickness of graphene). Let us denote the average out-of-plane velocity of carriers by $\bar{v}_z$. Following statistical theory of simple gases [46], the effusion rate (per unit area) of charge carriers in the direction $\hat{z}$ perpendicular to the graphene plane is given by

$$R = n_{3D} \int_{-\infty}^{+\infty} dv_x \int_{-\infty}^{+\infty} dv_y \bar{v}_z \mathcal{F}(\vec{v}) = n_{3D} \bar{v}_z, \tag{4}$$

where $n_{3D} = n_{2D}/l_\perp$ with n_{2D} being the number of carriers per unit area that contribute to the current flow across the Schottky barrier. Hence, statistical considerations for the 2D graphene sheet leads to

$$\mathcal{J}_0 = q n_{3D} \bar{v}_z = q \frac{n_{2D}}{l_\perp} \bar{v}_z. \tag{5}$$

From the band diagram shown in Fig. 2(a), the number of carriers overcoming the interface barrier reads

$$n_{2D} = \int_{\varphi_{B0}}^{\infty} \mathcal{D}(E) f_{FD}(E) dE. \tag{6}$$

Substituting the density of electronic states of graphene as $\mathcal{D}(E) = g_{sv} E / 2\pi \hbar^2 v_F^2$ and Fermi-Dirac distribution (f_{FD}), Eq. (5) readily leads to

$$\mathcal{J}_0 = \frac{\bar{v}_z}{l_\perp} \frac{q g_{sv} (k_B T)^2}{2\pi \hbar^2 v_F^2} \left(1 + \frac{q\varphi_{B0}}{k_B T}\right) \exp\left(-\frac{q\varphi_B}{k_B T}\right), \tag{7}$$

which is exactly the Ang-Yang-Ang equation for vertical graphene Schottky junction [20], which is originally derived from density-of-states' considerations.

2. Out-of-plane velocity of carriers in graphene

In the framework of the T^1 scaling law, the effective out-of-plane velocity and the Schottky barrier height can be determined experimentally from the activation-energy data of $\ln(|\mathcal{J}|T^{-1})$ vs $q/k_B T$ at reverse bias. Here, the slope and the intercept of regression line are equal to $-\varphi_B$ and $\ln(q\varphi_B \mathcal{C}_\mathcal{G} v_\perp^*)$, respectively. A typical T^1 scaling activation-energy data of the graphene-Si samples is shown in Fig. 3(a). The Schottky barrier height extracted from the slope of regression lines is determined as 0.40–0.43 eV, which is slightly lower than the barrier height obtained from the classical activation-energy plots [32]. Utilizing the barrier height extracted at a given bias voltage, we determine the effective out-of-plane velocity of carriers from the intercept of regression lines. As represented in Fig. 3(b), the average effective velocity of charge carriers across the G-Si(1) and G-Si(2) junctions are determined as $\langle v_\perp^* \rangle = 1.67(\pm 0.07)$ cm/s and $\langle v_\perp^* \rangle = 0.34(\pm 0.07)$ cm/s, respectively. Taking into account $v_\perp = 3.7 \times 10^8$ cm/s, we obtain nonconserving $\mathbf{k}_\parallel$ scattering strength as $\langle \lambda_{\mathbf{k}_\parallel} \rangle \approx 10^{-8}$, which is 4 orders of magnitude smaller that the previously determined scattering strength of $\lambda_{\mathbf{k}_\parallel} \approx 10^{-4}$ [20,43]. Later on, we show that this deviation can be attributed to the presence of an interfacial oxide layer at the graphene-silicon interface.

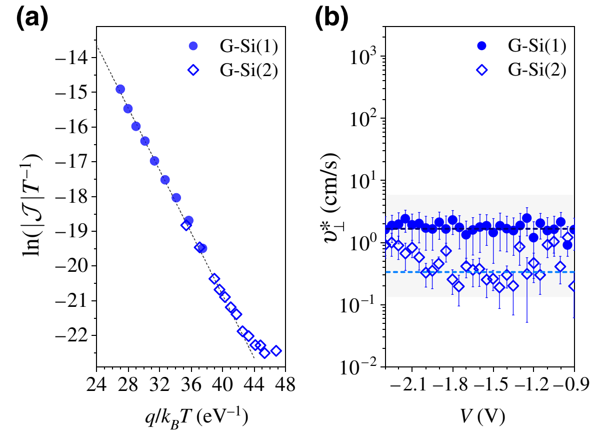

FIG. 3. (a) Activation energy of G-Si Schottky junctions with respect to the T^1 scaling law [Eq. (2)] at $V = -1$ V. (b) The effective out-of-plane velocity of charge carriers versus bias voltage.

C. Transfer velocity versus Schottky barrier height

In order to gain a general insight into the kinetics of charge carriers across the graphene-silicon Schottky junction, we analyze the activation-energy data from a variety of previous studies. For more information on the original data and the corresponding analyses see Sec. S2 within the Supplemental Material [32]. Figure 4 represents charge-carrier transfer velocity as a function of potential barrier at the graphene-Si interface. Practically, the transfer velocity varies almost exponentially with the Schottky barrier height. This is reasonable because to overcome a higher potential barrier, charge carriers have to possess a higher kinetic energy, whose distribution tail is almost exponential according to the Fermi-Dirac statistics. Intuitively, the data of Fig. 4 can be fitted by an exponential function

$$v = v_0 \exp(q\varphi_B / \mathcal{E}_{ch}), \tag{8}$$

where v_0 represents the minimum charge transfer velocity in the absence of potential barrier and $\mathcal{E}_{ch}$ is the characteristic kinetic energy of charge carriers. In the framework of classical thermionic emission theory [Fig. 4(a)], we obtain $\bar{v}_0 = 1.3 \times 10^{-4}$ cm/s and $\mathcal{E}_{ch} = 43.6$ meV. Similarly, utilizing the T^1 scaling law [Fig. 4(b)], the minimum effective velocity and characteristic kinetic energy of charge carriers

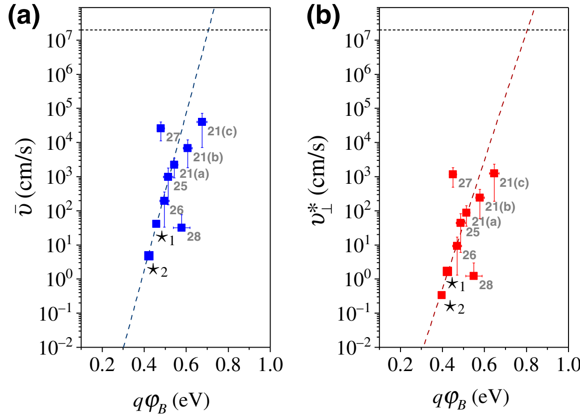

FIG. 4. Transfer velocity of charge carriers versus the Schottky barrier height across the graphene-silicon interface in the framework of (a) classical thermionic emission theory [Eq. (1)] and (b) T^1 scaling law [Eq. (2)]. The data are extracted by processing the activation-energy data of various studies whose reference numbers are shown next to the corresponding marks [32]. $\star_1$ and $\star_2$ indicate the data of G-Si(1) and G-Si(2) samples, respectively. Dashed lines represent fitted curves to the experimental data [Eq. (8)].

are obtained as $\upsilon_{\perp,0}^* = 4.1 \times 10^{-4}$ cm/s and $\mathcal{E}_{\text{ch}} = 53.2$ meV.

We note that although the transfer velocity increases with the Schottky barrier height, the number of charge carriers with higher kinetic energy is small, which means that the net current density declines. Combining Eqs. (2), (5), and (8), the density of charge carriers (contributing to the current flow) as a function of the effective out-of-plane velocity is given by

$$n_{2\text{D}}(\nu) = \frac{l_\perp}{q}\mathcal{C}_\mathcal{G} T\mathcal{E}_{\text{ch}}\left[\nu^{-\kappa}\ln(\nu)\right], \qquad (9)$$

where $\nu = \upsilon_\perp^*/\upsilon_{\perp,0}^*$ and $\kappa = \mathcal{E}_{\text{ch}}/k_B T$. Accordingly, at room temperature the density of charge carriers incorporated into the current flow across the interface barrier shrinks approximately with the inverse square of transfer velocity: $n_{2\text{D}} \propto (\upsilon_\perp^*)^{-2}$.

D. Oxide layer at the interface

It has been suggested that the low Richardson constant at the graphene-silicon interface can be explained within the framework of classical thermionic emission theory [Eq. (1)] if one takes into account a thin interfacial oxide layer, which can be grown during the wet transfer of CVD-graphene onto silicon surface [25,28,30]. We investigate the presence of silicon oxide at the graphene-silicon interface by x-ray photoelectron spectroscopy (XPS).

Figure 5(a) presents the survey spectrum of the graphene-silicon window where the dominant signals correspond to silicon, carbon, and oxygen core levels. The high-resolution carbon 1s spectrum is shown in Fig. 5(b) where the intense signal at 284.8 eV comes from sp^2 bonds. The shoulder at higher binding energy is well fitted by two Gaussian distributions centered at 286 and 288.7 eV, which can be attributed to C—O and C—N bonds, respectively [47,48]. Figure 5(c) shows the silicon 2s core level signal with the main peak at 150.9 eV. In the case of the H-terminated silicon surface, there should be only one peak related to elemental silicon (Si^0). The presence of SiO_2 (Si^{+4}) on the silicon surface induces an additional peak, which typically appears at $E_{\text{bind}}(\text{Si}^0_{2s}) + 3.7$ eV and the corresponding signals of silicon suboxides (SiO_x, $x < 2$) locate between Si^0 and Si^{+4} peaks [49]. In the case of graphene-silicon interface [Fig. 5(c)], the shoulder at higher energies is well modeled by a Gaussian centered at 153.9 eV, i.e., $E_{\text{bind}}(\text{Si}^0_{2s}) + 3.0$, which confirms the presence of SiO_x at the graphene-silicon interface. Similarly, in the presence of silicon oxide, the elemental peak of silicon 2p core level is accompanied by a shoulder at higher binding energies [50]. For the graphene-silicon interface, as represented in Fig. 5(d), the elemental peak of Si 2p core level at 99.7 eV appears alongside a shoulder centered at $E_{\text{bind}}(\text{Si}^0_{2p}) + 3.1$ eV. Hence, XPS spectra clearly confirm that the wet transfer of CVD-graphene onto H-terminated silicon and the subsequent heating procedure cause the silicon surface to be partly oxidized.

A thin insulating layer modifies the Richardson constant by a tunneling factor as $A_r^{**} = A^{**}\exp(-\delta\sqrt{\phi})$, where δ and ϕ are the average thickness of oxide layer (Å) and the effective tunneling barrier height (eV), respectively [51]. Applying a similar argument to Eq. (1), a thin interfacial oxide layer modifies the average transfer velocity as $\bar{\upsilon}_r = \langle\upsilon_{\text{th}}\rangle\exp(-\delta\sqrt{\phi})$. Considering $\bar{\upsilon}_r/\langle\upsilon_{\text{th}}\rangle = 2.17 \times 10^{-6}$ for G-Si(1), we determine the tunneling factor as $\delta\sqrt{\phi} = 13.04$, which implies an average oxide thickness of 32.6 Å [51,52].

E. Exponential dependence of $\lambda_{k_\parallel}$ on Schottky barrier height

Although the presence of an interfacial oxide layer certainly affects the injection velocity of charge carriers, the above picture of tunneling factor cannot explain the exponential dependence of velocity on the Schottky barrier height [Fig. 4(a)] implying the failure of classical thermionic emission theory at the 2D-3D graphene-silicon Schottky junction. T^1 scaling law [Eq. (2)], on the other hand, gives a thorough interpretation of experimental data provided that we consider the scattering strength

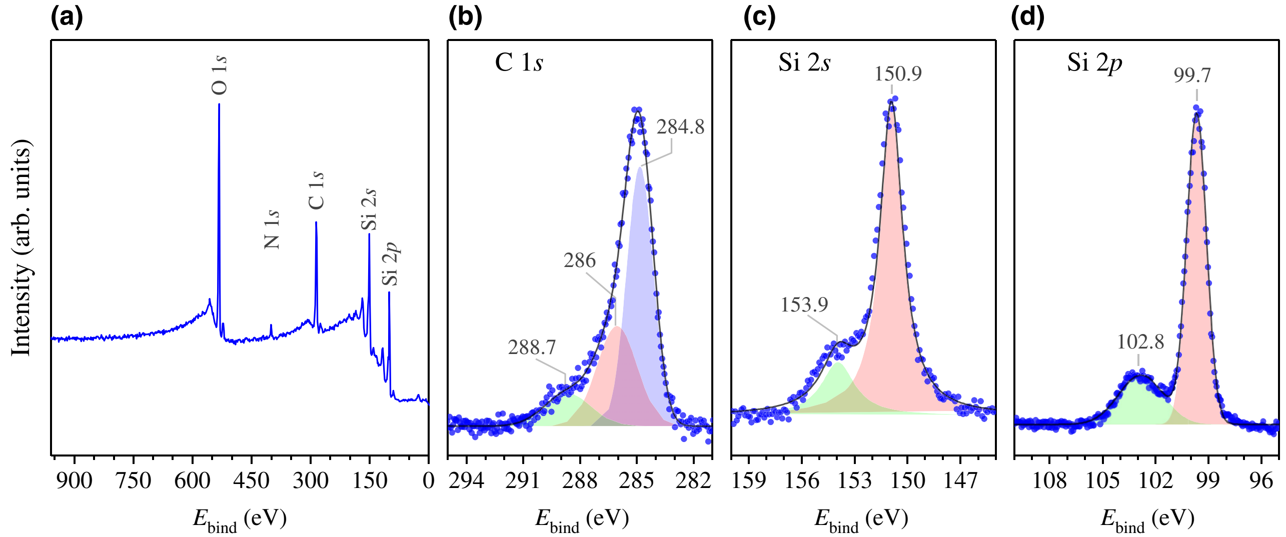

FIG. 5. X-ray photoelectron spectra of the graphene-Si interface. (a) Survey spectrum showing the elements present at the sample surface. (b)–(d) High-resolution spectra of carbon 1s, silicon 2s, and silicon 2p core levels. Black lines are cumulative fit curves.

of nonconserving lateral momentum as [Eq. (8)]

$$\lambda_{\mathbf{k}_\parallel} = \lambda^0_{\mathbf{k}_\parallel} \exp\left(\frac{q\varphi_B}{\mathcal{E}_{\rm ch}}\right), \tag{10}$$

where $\lambda^0_{\mathbf{k}_\parallel} \approx 1.1 \times 10^{-12}$, which also takes into account the effect of insulating interfacial layer. Combining Eqs. (10) and (2), we sum up the main conclusion of this study that the thermionic emission of charge carriers across the 2D-3D graphene-silicon Schottky junction is governed by

$$\mathcal{J}_0 = \lambda^0_{\mathbf{k}_\parallel} \frac{v_\perp q^2 g_{\rm sv}\varphi_{B0} k_B T}{2\pi l_\perp \hbar^2 v_F^2} \exp\left(\frac{q\varphi_B}{\mathcal{E}_{\rm ch}}\right) \exp\left(-\frac{q\varphi_B}{k_B T}\right). \tag{11}$$

IV. CONCLUSION

The transfer velocity of charge carriers across 2D-3D graphene-silicon Schottky junction is much smaller than the average thermal velocity of carriers in silicon, which is in sharp contrast to the normal 3D-3D Schottky junctions. This implies that charge transport across the graphene-silicon interface is substantially limited by the effective out-of-plane velocity of charge carriers in graphene. Our findings indicate that the average transfer velocity varies exponentially with the Schottky barrier height. The minimum transfer velocity and the characteristic kinetic energy of charge carriers contributing to the current flow are obtained as $v_0 \sim 10^{-4}$ cm/s and $\mathcal{E}_{\rm ch} \approx 50$ meV, respectively. It is also shown that statistical considerations of charge-carrier kinetics in two dimensions lead to the T^1 scaling formalism of thermionic emission at the vertical graphene-semiconductor Schottky junction. The classical theory of thermionic emission cannot explain the exponential dependence of charge-carrier velocity on the Schottky barrier height even if one takes into account the effect of the interfacial silicon suboxide layer at the graphene-silicon interface. The experimental data can be well interpreted within the framework of the T^1 scaling formalism [Eq. (11)] considering the exponential dependence of nonconserving lateral-momentum scattering strength on the interface barrier height. This exponential dependence can be understood based on the phenomenological arguments. However, its physical origin is not clear and requires extra theoretical investigations.

ACKNOWLEDGMENTS

The authors acknowledge “Iran’s National Elites Foundation (INEF)” Contract No. 15.10623 and “Iran Science Elites Federation (ISEF)” for financial support.

[1] K. Kim, J.-Y. Choi, T. Kim, S.-H. Cho, and H.-J. Chung, A role for graphene in silicon-based semiconductor devices, Nature **479**, 338 (2011).
[2] D. Akinwande, C. Huyghebaert, C.-H. Wang, M. I. Serna, S. Goossens, L.-J. Li, H.-S. P. Wong, and F. H. Koppens, Graphene and two-dimensional materials for silicon technology, Nature **573**, 507 (2019).
[3] S. Tongay, T. Schumann, and A. F. Hebard, Graphite based Schottky diodes formed on Si, GaAs, and 4h-SiC substrates, Appl. Phys. Lett. **95**, 222103 (2009).
[4] X. Li, H. Zhu, K. Wang, A. Cao, J. Wei, C. Li, Y. Jia, Z. Li, X. Li, and D. Wu, Graphene-on-silicon Schottky junction solar cells, Adv. Mater. **22**, 2743 (2010).
[5] R. Won, Graphene–silicon solar cells, Nat. Photonics **4**, 411 (2010).

[6] X. Li, Z. Lv, and H. Zhu, Solar cells: Carbon/silicon heterojunction solar cells: State of the art and prospects (adv. mater. 42/2015), Adv. Mater. **27**, 6767 (2015).
[7] S. K. Behura, C. Wang, Y. Wen, and V. Berry, Graphene–semiconductor heterojunction sheds light on emerging photovoltaics, Nat. Photonics **13**, 312 (2019).
[8] M. Javadi, Theoretical efficiency limit of graphene-semiconductor solar cells, Appl. Phys. Lett. **117**, 053902 (2020).
[9] S. Tongay, M. Lemaitre, X. Miao, B. Gila, B. R. Appleton, and A. F. Hebard, Rectification at Graphene-Semiconductor Interfaces: Zero-Gap Semiconductor-Based Diodes, Phys. Rev. X **2**, 011002 (2012).
[10] C.-C. Chen, M. Aykol, C.-C. Chang, A. F. J. Levi, and S. B. Cronin, Graphene-silicon Schottky diodes, Nano Lett. **11**, 5097 (2011).
[11] A. D. Bartolomeo, Graphene Schottky diodes: An experimental review of the rectifying graphene/semiconductor heterojunction, Phys. Rep. **606**, 1 (2016).
[12] H. Yang, J. Heo, S. Park, H. J. Song, D. H. Seo, K.-E. Byun, P. Kim, I. Yoo, H.-J. Chung, and K. Kim, Graphene barristor, a triode device with a gate-controlled Schottky barrier, Science **336**, 1140 (2012).
[13] M. Amirmazlaghani, F. Raissi, O. Habibpour, J. Vukusic, and J. Stake, Graphene-Si Schottky IR detector, IEEE J. Quantum Electron. **49**, 589 (2013).
[14] X. An, F. Liu, Y. J. Jung, and S. Kar, Tunable graphene–silicon heterojunctions for ultrasensitive photodetection, Nano Lett. **13**, 909 (2013).
[15] X. Liu, X. W. Zhang, Z. G. Yin, J. H. Meng, H. L. Gao, L. Q. Zhang, Y. J. Zhao, and H. L. Wang, Enhanced efficiency of graphene-silicon Schottky junction solar cells by doping with au nanoparticles, Appl. Phys. Lett. **105**, 183901 (2014).
[16] I. Goykhman, U. Sassi, B. Desiatov, N. Mazurski, S. Milana, D. de Fazio, A. Eiden, J. Khurgin, J. Shappir, U. Levy, and A. C. Ferrari, On-chip integrated, silicon–graphene plasmonic Schottky photodetector with high responsivity and avalanche photogain, Nano Lett. **16**, 3005 (2016).
[17] A. D. Bartolomeo, G. Luongo, L. Iemmo, F. Urban, and F. Giubileo, Graphene–silicon Schottky diodes for photodetection, IEEE Trans. Nanotechnol. **17**, 1133 (2018).
[18] X. Wang, Z. Cheng, K. Xu, H. K. Tsang, and J.-B. Xu, High-responsivity graphene/silicon-heterostructure waveguide photodetectors, Nat. Photonics **7**, 888 (2013).
[19] X. Li, L. Tao, Z. Chen, H. Fang, X. Li, X. Wang, J.-B. Xu, and H. Zhu, Graphene and related two-dimensional materials: Structure-property relationships for electronics and optoelectronics, Appl. Phys. Rev. **4**, 021306 (2017).
[20] Y. S. Ang, H. Y. Yang, and L. Ang, Universal Scaling Laws in Schottky Heterostructures Based on Two-Dimensional Materials, Phys. Rev. Lett. **121**, 056802 (2018).
[21] D. Sinha and J. U. Lee, Ideal graphene/silicon Schottky junction diodes, Nano Lett. **14**, 4660 (2014).
[22] Y. Xu, C. Cheng, S. Du, J. Yang, B. Yu, J. Luo, W. Yin, E. Li, S. Dong, P. Ye, and X. Duan, Contacts between two- and three-dimensional materials: Ohmic, Schottky, and *p–n* heterojunctions, ACS Nano **10**, 4895 (2016).
[23] S.-H. Tsai, S. Lei, X. Zhu, S.-P. Tsai, G. Yin, X. Che, P. Deng, J. Ng, X. Zhang, W.-H. Lin, Z. Jin, H. Qasem, Z. Zhou, R. Vajtai, N.-C. Yeh, P. Ajayan, Y.-H. Xie, and K. L. Wang, Interfacial states and Fano–Feshbach resonance in graphene–silicon vertical junction, Nano Lett. **19**, 6765 (2019).
[24] X. Zhu, S. Lei, S.-H. Tsai, X. Zhang, J. Liu, G. Yin, M. Tang, C. M. Torres, A. Navabi, Z. Jin, S.-P. Tsai, H. Qasem, Y. Wang, R. Vajtai, R. K. Lake, P. M. Ajayan, and K. L. Wang, A study of vertical transport through graphene toward control of quantum tunneling, Nano Lett. **18**, 682 (2018).
[25] Y. An, A. Behnam, E. Pop, and A. Ural, Metal-semiconductor-metal photodetectors based on graphene/*p*-type silicon Schottky junctions, Appl. Phys. Lett. **102**, 013110 (2013).
[26] D. Tomer, S. Rajput, L. J. Hudy, C. H. Li, and L. Li, Inhomogeneity in barrier height at graphene/Si (GaAs) Schottky junctions, Nanotechnology **26**, 215702 (2015).
[27] A. D. Bartolomeo, F. Giubileo, G. Luongo, L. Iemmo, N. Martucciello, G. Niu, M. Fraschke, O. Skibitzki, T. Schroeder, and G. Lupina, Tunable Schottky barrier and high responsivity in graphene/Si-nanotip optoelectronic device, 2D Materials **4**, 015024 (2016).
[28] A. D. Bartolomeo, G. Luongo, F. Giubileo, N. Funicello, G. Niu, T. Schroeder, M. Lisker, and G. Lupina, Hybrid graphene/silicon Schottky photodiode with intrinsic gating effect, 2D Materials **4**, 025075 (2017).
[29] J. Courtin, S. L. Gall, P. Chrétien, A. Moréac, G. Delhaye, B. Lépine, S. Tricot, P. Turban, P. Schieffer, and J.-C. L. Breton, A low Schottky barrier height and transport mechanism in gold–graphene–silicon (001) heterojunctions, Nanoscale Adv. **1**, 3372 (2019).
[30] G. Luongo, A. Grillo, F. Urban, F. Giubileo, and A. D. Bartolomeo, Effect of silicon doping on graphene/silicon schottky photodiodes, Mater. Today: Proc. **20**, 82 (2020).
[31] M. Javadi, A. Noroozi, A. Mazaheri, and Y. Abdi, Sequentially assembled graphene layers on silicon, the role of uncertainty principles in graphene–silicon Schottky junctions, Adv. Opt. Mater. **7**, 1900470 (2019).
[32] See Supplemental Material at http://link.aps.org/supplemental/10.1103/PhysRevApplied.14.064048 for optical figures, Schottky barrier height, and activation-energy data.
[33] E. H. Rhoderick and R. H. Williams, *Metals Semiconductor Contacts* (Oxford University Press, New York, USA, 1988), p. 95
[34] S. Sze and K. K. Ng, *Physics of Semiconductor Devices* (John Wiley & Sons, Inc., New Jersey, USA, 2006), p. 157
[35] Y.-J. Yu, Y. Zhao, S. Ryu, L. E. Brus, K. S. Kim, and P. Kim, Tuning the graphene work function by electric field effect, Nano Lett. **9**, 3430 (2009).
[36] M. Trushin, Theory of thermionic emission from a two-dimensional conductor and its application to a graphene-semiconductor schottky junction, Appl. Phys. Lett. **112**, 171109 (2018).
[37] M. Trushin, Theory of photoexcited and thermionic emission across a two-dimensional graphene-semiconductor Schottky junction, Phys. Rev. B **97**, 195447 (2018).
[38] S.-J. Liang, B. Cheng, X. Cui, and F. Miao, Van der waals heterostructures for high-performance device applications:

Challenges and opportunities, Adv. Mater. **32**, 1903800 (2019).

[39] S. Banerjee, L. Cao, Y. S. Ang, L. Ang, and P. Zhang, Reducing Contact Resistance in Two-Dimensional-Material-Based Electrical Contacts by Roughness Engineering, Phys. Rev. Appl. **13**, 064021 (2020).

[40] S.-J. Liang and L. K. Ang, Electron Thermionic Emission from Graphene and a Thermionic Energy Converter, Phys. Rev. Appl. **3**, 014002 (2015).

[41] Y. Ang and L. Ang, Current-Temperature Scaling for a Schottky Interface with Nonparabolic Energy Dispersion, Phys. Rev. Appl. **6**, 034013 (2016).

[42] Y. Ang, S.-J. Liang, and L. Ang, Theoretical modeling of electron emission from graphene, MRS Bulletin **42**, 505 (2017).

[43] Y. S. Ang, Y. Chen, C. Tan, and L. K. Ang, Generalized High-Energy Thermionic Electron Injection at Graphene Interface, Phys. Rev. Appl. **12**, 014057 (2019).

[44] D. Vashaee and A. Shakouri, Electronic and thermoelectric transport in semiconductor and metallic superlattices, J. Appl. Phys. **95**, 1233 (2004).

[45] D. Vashaee and A. Shakouri, Improved Thermoelectric Power Factor in Metal-Based Superlattices, Phys. Rev. Lett. **92**, 106103 (2004).

[46] R. K. Pathria and P. D. Beale, *Statistical Mechanics* (Elsevier Ltd, Oxford, UK, 2011), 3rd ed., p.152

[47] Y.-S. Ye, Y.-N. Chen, J.-S. Wang, J. Rick, Y.-J. Huang, F.-C. Chang, and B.-J. Hwang, Versatile grafting approaches to functionalizing individually dispersed graphene nanosheets using RAFT polymerization and click chemistry, Chem. Mater. **24**, 2987 (2012).

[48] Y. Liu, L. Yuan, M. Yang, Y. Zheng, L. Li, L. Gao, N. Nerngchamnong, C. T. Nai, C. S. S. Sangeeth, Y. P. Feng, C. A. Nijhuis, and K. P. Loh, Giant enhancement in vertical conductivity of stacked CVD graphene sheets by self-assembled molecular layers, Nat. Commun. **5**, 5461 (2014).

[49] T. Bekkay, E. Sacher, and A. Yelon, Surface reaction during the argon ion sputter cleaning of surface oxidized crystalline silicon (111), Surf. Sci. **217**, L377 (1989).

[50] F. J. Himpsel, F. R. McFeely, A. Taleb-Ibrahimi, J. A. Yarmoff, and G. Hollinger, in *The Physics and Chemistry of SiO2 and the* Si-SiO2 *Interface* (Springer, US, 1988), p. 219.

[51] H. C. Card and E. H. Rhoderick, Studies of tunnel MOS diodes i. interface effects in silicon Schottky diodes, J. Phys. D: Appl. Phys. **4**, 1589 (1971).

[52] M. Javadi, A. Mazaheri, H. Torbatiyan, and Y. Abdi, Mechanism of Charge Transport in Hybrid Organic-Inorganic PEDOT:PSS/silicon Heterojunctions, Phys. Rev. Appl. **12**, 034002 (2019).